JOURNAL OF PROPULSION AND POWER
Vol. 24, No. 2, March–April 2008

Strongly Swirling Turbulent Sink Flow Between Two Stationary Disks

G. H. Vatistas,* M. Fayed,† and J. U. Soroardy‡
Concordia University, Montreal H3G 1M8, Canada

DOI: 10.2514/1.29618

The steady, incompressible turbulent sink flow developing between two stationary disks under the influence of strong swirl was numerically investigated. The simulations were made using the FLUENT 6.2 software. The purpose of the study is to first validate the method and then proceed in identifying the origin of some key known flow features, such as the appearance of a toroidal recirculation zone in the central flow region, the saddlelike behavior of the tangential velocity, and the two radial velocity kinks near the two end plates. The simulations are found to be in good accord with earlier experiments. Centrifugal force is shown to be the prime culprit for all of the previous flow manifestations. The overpowering centrifugal force compels the fluid to drain mainly through the end-plate boundary layers where its value is the minimum. The buildup of the recirculation zone is a natural response by the fluid to account for the local flow inactivity. This buildup is also responsible for the evolution of a weak reversed flow in the midchannel plane that, along with turbulence and the nonslip condition on the disk surface, produces the until-now unexplained saddlelike shape of the tangential velocity profile. The growth of the radial velocity spikes near the disks is due to the synergetic action of the boundary-layer development and the reduction of the local flow area. Finally, the simulations have also unveiled a previously unknown tangential velocity undulation inside the vortex core triggered by vortex transition from laminar to turbulent conditions.

Nomenclature

H	=	exit length port, m
h	=	gap size, m
p	=	static pressure, Pa
p_{in}	=	inlet static pressure, Pa
Q	=	volume flow rate, m^3/kg
R_o	=	radius of the disc, m
R_i	=	radius of sink exit, m
r, θ, z	=	polar coordinates; m, rad, m
r_c	=	vortex core radius, m
S	=	swirl ratio, $V_{\theta\text{in}}/V_{r\text{in}}$
V	=	dimensionless swirl velocity, $V_\theta \xi_c / V_{\theta\text{in}}$
V_r	=	radial velocity, m/s
$V_{r\text{in}}$	=	inlet radial velocity, m/s
V_θ	=	swirl or tangential velocity, m/s
$V_{\theta\text{in}}$	=	inlet swirl velocity, m/s
$\Delta\Pi$	=	dimensionless pressure, $(p - p_{\text{in}})/\rho V^2_{\theta\ \text{in}}$.
ζ	=	dimensionless axial coordinate, z/h
μ	=	dynamic viscosity of fluid (air), $N \cdot s/m^2$
μ_t	=	turbulence viscosity, $N \cdot s/m^2$
ξ	=	dimensionless radial coordinate, r/R_o
ξ_c	=	dimensionless vortex radius, r_c/R_o
σ	=	aspect ratio, $h/2R_o$

I. Introduction

THE strongly swirling inflow in shallow disklike domains remains an outstanding problem since the early 1960s. This type of a problem can also be viewed as flow in a short cyclone chamber. Contributions to the general subject were mainly the result of the gaseous nuclear rocket motor project [1], the vortex fluidic device [2], the vortex separator and combustor [3–5], and the Ranque–Hilsh [6,7] tube refrigerator [8].

The gas core nuclear reactor rocket of the 1960s features a conceptual type of propulsion system whereby a vehicle could be propelled in space using the hot gases produced by cooling nuclear fissile materials [9]. The idea is based on the realization that the energy density in such environments is considerably higher (8.37×10^{10} kJ/kg) compared with the conventional chemical reaction counterpart [10] (12.56×10^3 kJ/kg). Therefore, the rocket is theoretically capable of delivering a much higher specific impulse and thrust than most of the chemical motor designs. Following a decade of development, the engine was designed and built. Ground tests showed that the propellant could achieve almost double the exhaust gas velocity than that provided by the traditional chemical rocket [10]. Because of these attractive characteristics, space vehicles using this principle would have greatly advanced the potential of space travel [9]. However, probably due to the then material limitations on the temperature [10], the project was discontinued. Based on the progress made on new material and flow computational capabilities in the last 50 years the project may be resurrected. Nevertheless, the environmental issue of how to safely transport highly radioactive material into space must also be convincingly addressed.

Two fundamentally different types of flows could evolve between two parallel disks. Forcing the fluid to enter through the periphery and to drain through a centrally located exit located on one or on both disks produces a sink or converging flow. Reversing the direction of the last type, keeping in mind that reversing the flow direction may not always reverse the flow characteristics, can create a source flow. Both inflow and outflow exhibit the phenomenon of relaminarization [11]. Superimposing swirl at the inlet will then give rise to converging and diverging vortex flows, respectively. The presence of the tangential velocity component produces a strong centrifugal field, which radically alters the character of the fluid motion. Flows of this kind are routinely encountered in a number of standard technological applications, such as radial diffusers, flow regulating valves, multiple-disk turbo-machinery components, air bearings, disk-type heat exchangers, pneumatic micrometers, flow and viscosity meters, and many others.

Past experimental, theoretical, and numerical efforts approached the general problem from different angles with the aim of examining

Received 6 January 2007; accepted for publication 16 November 2007.

*Professor, Mechanical and Industrial Engineering Department, 1455 De Maisonneuve Boulevard West. Senior Member AIAA

†Ph.D. Candidate, Mechanical and Industrial Engineering Department, 1455 De Maisonneuve Boulevard West.

‡M.A.Sc. Student, Mechanical and Industrial Engineering Department, 1455 De Maisonneuve Boulevard West.

some specific flow characteristics. The complexities associated mainly with the dominance of the centrifugal force and the complexities of the boundary conditions introduce severe obstacles that have prevented a general analytical solution in the past. Furthermore, an excessive time (and thus prohibitive cost) requirement had also hindered even a proper experimental characterization of the problem. Computer capacity limitations did not permit a refined numerical approximation; see, for example, Gupta et al. [5] and Vatistas [12]. The rapid advances in computer hardware and software technology have encouraged us to revisit the problem and solve numerically the turbulent swirling flow using the commercially available computational fluid dynamics (CFD) software FLUENT 6.2.

In the last few decades a large number of analytical, numerical, and experimental investigations have improved our understanding of the general phenomenon. Because papers dealing with the general theme are vast, priority will only be given here to contributions that are directly relevant to the present work. Therefore, only work done in the low aspect ratio range under the influence of strong swirl or those that deal with the aforementioned unexplained phenomena will be mentioned. Hence, the relatively brief literature review provided here is rather indicative than exhaustive. More details on the focused theme can also be found in the fine contributions of Lewellen [10], Gupta et al. [5].

Motivated by the gas core nuclear reactor rocket program, Savino and Keshok [13] conducted a series of experiments in a 0.107 aspect ratio cylindrical chamber under the influence of a strong swirl, with the aim to map the radial, tangential velocity, and pressure distributions. The causes that had as an effect the development of the particular velocity and pressure profiles were examined. Air was injected tangentially through the periphery and exhausted through a centrally located outlet. A probe was used to sense both the magnitude and direction of the velocity at different radial locations. The nondimensional radial velocity profiles were found to exhibit a distinct similarity near the upper and lower boundaries (top and bottom plates). It was discovered that under the influence of a strong centrifugal field the fluid finds the exit moving close to the upper and lower disks where, due to the presence of the boundary layers, the centrifugal force is at its minimum. Consequently, the fluid choosing the path of least resistance is seen to find the exit flowing along the upper and lower plates. In the midchannel region, the measurements revealed that the radial velocity was small. Relatively far from the exit port and near the midchannel, the tangential velocity closely followed a free-vortex profile. This hypothesis made the analytical determination of the pressure possible within a limited range of the radius. The determining factor responsible for such behavior is strong inlet swirl ($S = 15$ in their case).

The first CFD simulation using the finite differences technique was made by Hornbeck [14]. His mathematical model presumed a steady, incompressible, laminar, axi-symmetric flow. The set of equations chosen to describe the fluid motion were momentum in the radial and tangential directions (with the viscous terms in the radial coordinate neglected) and continuity. The bulk conservation of mass was used to close the system. Because of the numerical instability of the scheme, when radial flow reversal was present, no comparisons were made with the detailed experimental data of Savino and Keshok [13].

Wormley [15] developed a momentum integral analysis for a steady, incompressible swirling inflow in a short vortex valve by considering the interaction between the inviscid vortex core and the viscous end-wall boundary layers. The inlet and exit regions of the chamber were excluded. In search of simplifying assumptions for the analytical solution, a series of water flow visualizations were also performed employing air bubbles and milk powder to see the flow. In the experiment, the steady stream of bubbles entered the chamber and immediately rose to the upper wall and then traveled to the exit closely following the upper disk surface. At a very high swirling ratio, the milky donutlike pattern lingered for a long time near the midplane of the chamber, indicating the existence of a lesser radial flow region, with the bulk of the fluid moving mainly through the end-wall boundary layers. As the swirl strength was reduced, the radial flow penetrated further into the midchannel plane. At very weak swirl, the milky pattern disappeared, confirming that a radial flow was developing along the entire axial span of the chamber. In his analytical modeling, he divided the flow into two flow regions: the developing and developed. Each region was further subdivided into two zones: the boundary layer and core flow. In midchannel, both the radial and tangential velocities were assumed to be the sole functions of the radius, whereas, near the end walls, they also were functions of the axial coordinate. The obtained analytical expression for the pressure variation agreed well with the experimental findings. A parameter identified as the boundary-layer coefficient, a function of the valve diameter, peripheral flow, total flow, and the wall friction factor, was derived for short vortex valves.

Based on Wormley's technique [15], Kwok et al. [16] numerically solved a set of differential equations for the flow within the annular region of a short vortex chamber. The purpose of the their work was to extend Wormley's methodology by examining the flow development as well as the variation of the apparent viscosity throughout the flowfield. Assuming the apparent viscosity (eddy plus the operating viscosity) to be a function of the tangential velocity in the core, the governing equations were simplified and integrated. Their calculations showed the nondimensional boundary-layer thickness of the entering fluid to first increase, reaching a maximum, and then reduce as the flow approached the sink. The tangential and radial velocity profiles agreed well to some extent with the experiment within the main chamber. Near the exit where the streamlines bend to find the exit, the agreement was unsatisfactory. Furthermore, the simulation results showed that the radial velocity is not resolved adequately in both of the boundary layers and inside the core flow regions. An empirical equation for the apparent viscosity was also derived.

Recently, a method for determining the compressible turbulent flow in a short vortex chamber was presented by Sorokin [17]. Their approach involved the calculations of the end wall boundary layers via the integral method and the flow discharge under the hypothesis of an ideal atomizer.

The aforementioned deficiencies in past theoretical representations encouraged us to embark on a more detailed flow examination, via numerical means, of a phenomenon relevant to both science and technology. In this paper we present numerical solutions of strongly swirling turbulent sink flows, which evolve within the small aperture formed by two stationary parallel disks. It is shown that commercial CFD packages, such as FLUENT, can indeed adequately resolve the most salient characteristics of the problem. FLUENT provided an economical method to identify the cause of the previously experimentally well-known kinks of the tangential and radial velocity components (near the two end plates). It was also able to identify an unexpected mode change for the swirl velocity inside the vortex core. Through simulations, the cause of this effect is shown to be the flow reversion from turbulent to laminar vortex conditions. The present contribution furnishes a validated method with which one can probe deeper into the physics of flows of this kind.

II. Problem and Numerical Technique

The inward swirling fluid motion developed within the gap formed by placing two coaxial parallel disks one on top of the other is considered here (see Fig. 1). A centrally located outlet, having the shape as a cylindrical manifold, is fitted onto the upper plate. The flow developed is assumed to be steady, incompressible, and turbulent. The mathematical representation of the present problem follows the usual approach, in which the phenomenon is supposed to be described by the full conservation equations of continuity and momentum together with the transport equations for the Reynold's stresses that are required to close the system. The following will be discussed later in the paper: a) the choice of the numerical model, b) the grid, c) the imposition of the boundary conditions, and d) the solution procedure used to simulate the problem.

Selection of the turbulence model depends strongly on the physics of the flow under consideration, and no universal model can be adopted. In addition to severe streamline bending near the exit

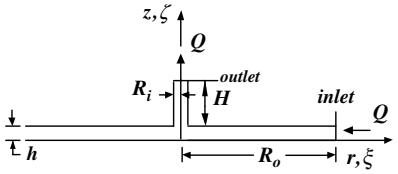

Fig. 1 Schematic of the problem.

expected here, the experiments of Savino and Keshok [13] have revealed the occurrence of a toroidal recirculation zone in the midchannel region, which further exacerbates the situation. It is for this reason that in the present study the Reynolds stress model (RSM) was employed. Other approaches, such as the k–ε mode are only appropriate for cases in which there is either no or weak streamline twist. Otherwise, the RSM's five equations for a two-dimensional problem and seven equations for a three-dimensional geometry are known to accurately predict the flow characteristics. The swirl ratio (S) is the factor that guides one in the selection of the most appropriate turbulence model. It is suggested that when highly swirling flow ($S > 0.5$) is present, as is the case for the present problem, the k–ε model will not accurately describe the flow. Our exploratory tests using the k–ε methodology reconfirmed the validity of the recommendation. Runs using the previous turbulence model produced either unrealistic results for low swirl or, in the case of high swirl, resulted in a nonconverging algorithm.

The mathematical modeling and solution methodology of the present problem was done using the FLUENT 6.2 approach [18]. No alterations to the original code, including the values of all coefficients, were made.

Preprocessing includes a clear definition of the physical problem that requires a solution, the selection of suitable flow domain geometry, optimum mesh generation, and the setting up of appropriate boundary conditions.

In the experimental settings of Savino and Keshock [13], the outer radius for both disks was $R_o = 14.88$ cm, the radius of the outlet manifold was $R_i = 2.54$ cm, and the gap depth was taken to be $h = 3.175$ cm. The inlet mass flow rate was the same as in the previous experiments ($m^o = 0.0948$ kg/s).

Because the present is a case of strongly swirling flow that involves steep velocity and pressure gradients, sufficient grid resolution is required for an accurate representation of the fluid properties. Because the flow was assumed to be axisymmetric, a two-dimensional geometry was sufficient in representing the entire domain. In the present study, the quadrilateral mesh was employed because it offers many advantages over the triangular for simple and moderately complex shapes. In some situations, quadrilateral elements lead to less expensive computations as they permit a much larger aspect ratio than their triangular counterparts. In addition, the large aspect ratio of a triangular cell can affect its skewness, which may produce inaccuracies in the solution and even hinder the convergence of the algorithm. Therefore, for relatively simple geometry as is the case with the present problem, the quadrilateral mesh is recommended. The grid size used for the productive runs was obtained by parametric studies that examined the effects of the size on the solution. The result of this study at one of the positions ($\zeta = 0.5$ and $\zeta = 0.51$) is shown in Figs. 2a and 2b. A grid size of 0.45 mm was found to provide an acceptably good solution to the problem. Note that if a 0.41 mm size was used instead the percentage difference in the results would have been less that 0.15%. To ensure good quality simulations, especially at this critical position where the fluid experiences a steep velocity gradient, a uniform mesh was adopted, with a finer mesh overlaid near the boundary walls.

Selecting the appropriate boundary conditions for the domain is a very important step in modeling. Four different conditions were applied at the domain's boundaries; these were the inlet, wall, axis, and outflow boundary conditions.

The inlet boundary condition involves the imposition of the velocity along with the values of all relevant scalar properties of the flow at the entrance of the domain. The axial velocity component was taken to be zero. The radial was obtained from the mass flow rate,

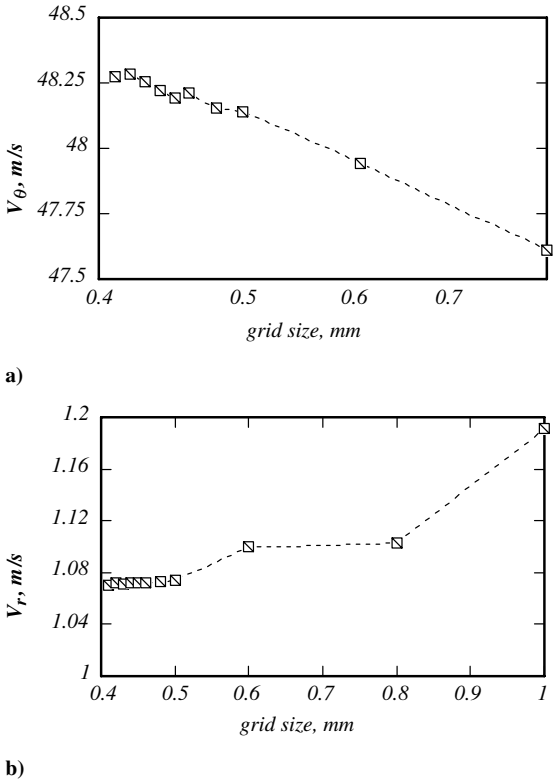

Fig. 2 Influence of grid size on velocity components at $\zeta = 0.5$ and $\zeta = 0.51$: a) swirl, and b) radial.

whereas the tangential velocity was imposed. Assuming a uniform inlet velocity may lead to an improper boundary condition that may affect the solution. Using the experimental velocity profile at the inlet is the most appropriate; unfortunately, it was not provided by Savino and Keshock [13]. To better meet the requirement, the diameter of the discs was appropriately extended and then a uniform radial velocity was imposed.

Turbulent intensity and the hydraulic diameter specification method are strongly recommended to model internal turbulent flows. The sensitivity of the solution to the inlet turbulence intensity was examined and found to have no significant influence on the solution. The hydraulic diameter was set to be twice the disk spacing ($D_H = 2h$).

The standard wall boundary condition is used for all the solid surfaces: a) $z = 0$, $r \geq 0$, for any θ; b) $z = h$, $r > R_i$, for any θ; and c) $h < z < (h + H)$, $r = R_i$ for any θ.

The impermeability and nonslip conditions for the velocity were used. All the other properties associated with the velocity components were assumed to be to be zero.

The axis boundary type must be used at the centerline of the axisymmetric geometry, which is achieved in FLUENT by default. The outflow condition in this software is used to model flow exits for which the details of velocity and pressure are not known before the solution. The solver extrapolates the required information from the interior points. Extra care must be taken when using these types of boundary conditions. They should not be applied in cases in which reversed flow is anticipated. Therefore, in our problem the exhaust manifold was extended past the vena contracta. A length H of 5 cm was found to be sufficient in avoiding this difficulty. Our preliminary tests have shown that failing to mind this problem will produce discrepancies in the velocity and pressure calculations.

The semi-implicit method for pressure-linked equations scheme was chosen for the pressure–velocity coupling. A second-order upwind discretization for the momentum equations, swirl velocity, turbulence kinetic energy, turbulence dissipation rate, and Reynolds stresses was set to reduce numerical diffusions. To achieve convergence, the default settings with underrelaxation factors of 0.3, 0.7, 1, 1, 0.9, 0.8, 0.8, 1, and 0.5 for the pressure, momentum,

density, body force, swirl velocity, turbulent kinetic energy, turbulent dissipation rate, turbulent viscosity, and Reynolds stresses were used, respectively.

III. Analysis of Results

The experimental arrangement of Savino and Keshock [13] is the starting point of the present numerical simulations, in which the problem can be viewed either as swirling flow between two disks with a small separation or the flow in a very short cyclone chamber.

A singular characteristic of flows of this kind is the development of a toroidal recirculation zone, which covers a hefty part of the main flow area (see Fig. 3). The presently calculated streamline patterns shown in Fig. 3 resemble intimately those obtained experimentally by Savino and Keshock [13] (see their Fig. 6). As the fluid enters the domain, it immediately senses the centrifugal force. In the attempt to find the exit taking a path of least opposition, it splits into two streams. The first stream flows along the upper plate while the second one propagates next to the lower disk. Because the viscous fluid must meet the nonslip boundary condition on the solid surfaces the centrifugal force in these regions is at its minimum. Streamline contraction in the proximity of the walls points out that most (if not all) of the inlet flow finds the exit moving through the top and bottom layers. Flow visualizations by Wormley [15] in a short vortex valve also revealed the preference of the radial to find the exit through the boundary layers. Photographs with injected milky powder have shown that the higher the swirl number, the smaller the portion of the fluid that finds the exit through a midchannel path. When the swirl ratio was decreased, more of the radial component was penetrating the midgap, causing the milky donutlike (toroidal recirculation) zone to occupy a lesser portion of the central area of the chamber. At the lowest swirl ratio, there was no donutlike flow region remaining in the domain.

Because most of the fluid finds the exit through the two boundary layers, the buildup of the toroidal recirculation zone at the central portion of the gap is a natural response by the fluid to adjust for the local flow inactivity. Both the present simulations (see Fig. 3) and the experiments by Savino and Keshock [13] (see their Fig. 6) show two counter-rotating vortices dwelling inside the flow recirculation area. The reason is that a counter-rotating pair is required to match simultaneously the direction of both the upper and lower streams. The aforementioned recirculation area is seen to extend up to the inlet and to even penetrate deep into the exit region. Savino and Keshock [13] conducted their experiments under one swirl ratio ($S = 15$). Here, the numerical results in terms of the radial and tangential components along with the pressure profiles will be compared with their experimental counterparts [13].

The radial velocity profiles obtained numerically and experimentally are shown in Figs. 4a–4f. Considering the complexity of the problem, the correlation between the two is quite good. The familiar peaks in the proximity of the disks, revealing the presence of strong inward radial streams [13,19], is very evident. Because of the reduction of the cross-sectional flow area, in the streamwise direction "the spikes increased in magnitude with decreasing radius" as was noted by Savino and Keshock [13]. The presence of the toroidal recirculation zone in the middle of the channel is the cause of flow reversal.

These figures show an overall good agreement between the experimental data and the numerical simulations. As expected, none of the previously mentioned theories were able to match the level of refinement of the present approach. Therefore, the present solutions are the first simulations that describe this phenomenon with a respectable degree of detail. However, small differences near the boundary wall and in the vicinity of the exit do exist. The disparities near the wall may be due to probe interference. The differences near the exit were anticipated. In the present numerical simulation, we are assuming constant density flow. Because of the pressure variation along the radius a density change is expected, particularly in the neighborhood of the exit where the static pressure drops rapidly. Note that Savino and Keshock [13] reported an overall experimental density variation of 10% along the radius that has not been taken into consideration here.

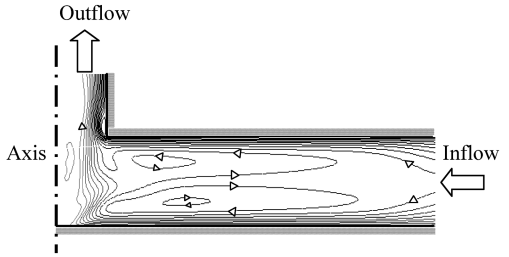

Fig. 3 Typical streamline patterns in the meridional plane.

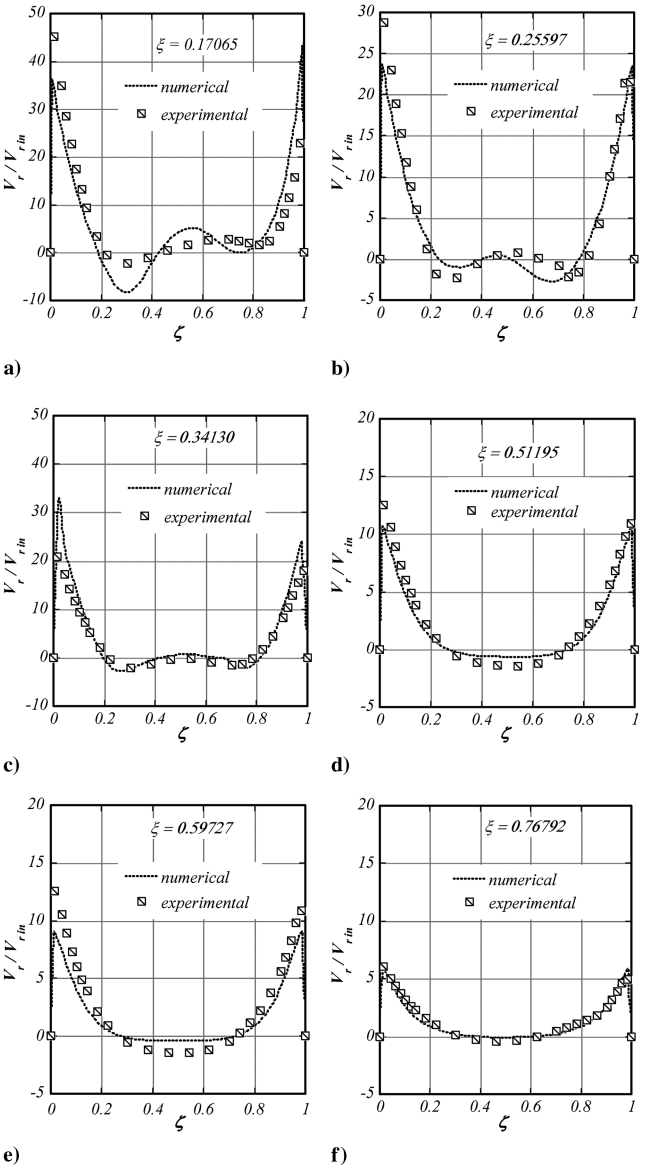

Fig. 4 Radial velocity axial profiles at seven different radial locations: a) velocity distribution near the exit, b) velocity distribution at approximately midradius point, and f) velocity distribution near the inlet. The experimental data are taken from Savino and Keshock [13].

Following the validation of the method, we then proceed to explain some of the very basic characteristics concerning the nature of the problem and attempt to provide answers to some outstanding questions. Because the turbulent viscosity calculations do take into consideration the fluctuating components of the flow, such as the Reynolds stresses, we have elected to examine the phenomenon using the more physical parameter μ_t in lieu of the customary turbulent quantities.

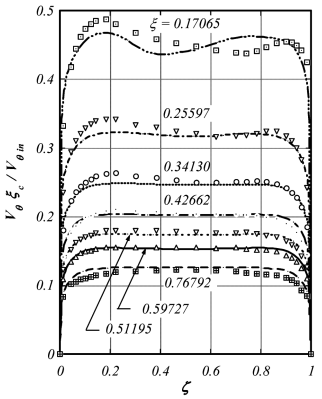

Fig. 5 Tangential velocity profiles. Symbols and curves represent the experimental data [13] and the present numerical simulations, respectively.

The axial variation of the tangential velocity for seven radial stations is given in Fig, 5. It is clear from both the numerical and experimental profiles that the velocity component, for the most part, exhibits a saddlelike behavior, with minimum values occurring near the midchannel region accompanied by two overshoots near the end plates. Next, we will examine the cause behind this unusual velocity manifestation.

Along the radius, the numerically calculated midchannel tangential velocity variation, together with the latest turbulent vortex approximation [20],

$$V = \frac{7.93\xi}{\{0.92 + (10\xi)^4\}^{0.48}} \tag{1}$$

and the experimental data of Savino and Keshock [13] are presented in Fig. 6. The laminar $n = 2$ vortex approximation,

$$V = \frac{10\xi}{\{1 + (10\xi)^4\}^{1/2}} \tag{2}$$

is also included [21]. Rankine's free-forced vortex does envelope the present numerical results. However, the free and forced vortex modes are approached by the real flow asymptotically as $\xi \to 1$ and 0, respectively. Besides the apparent kink of the velocity close to the axis of rotation (that we will revisit later on), the turbulent approximation accurately describes the numerical simulations. The laminar approximation is seen to overestimate the actual velocity. As mentioned previously, the numerically obtained values of the turbulent viscosity are good indicators with which one can gauge the turbulent intensity. The axial distribution of the normalized turbulent viscosity for four radial stations is given in Fig. 7. The axial location where maximum turbulence occurs is indicated in Fig. 8 by curve A.

In the previous experimental investigations by Kendall [19] and Savino and Keshock [13], the saddlelike behavior of the tangential velocity in the middle of the channel and the two crests near the boundary layers were very apparent. This result was unexpected and compelled the Kendall [19] to remark, "the cause of the tangential velocity overshoot has not been explained." Let us consider for example radial station $\xi = 0.59727$ in conjunction with Fig. 5. From Fig. 7, we see that the maximum turbulence occurs when $\zeta \approx 0.5$. There, from Fig. 6, the velocity must be at its minimum value. Moving now, say, toward the upper plate, the normalized viscosity drops indicating that turbulence decreases. Consequently, the velocity, from Fig. 6, must be heading in the direction of the $n = 2$ laminar-vortex profile or, in other words, increase. This augmentation, however, cannot persist indefinitely because at an appropriate value of ζ, the velocity should begin to reduce to meet the nonslip boundary condition on the upper disk surface. A similar sequence of events is taking place on the lower portion of the channel. This state of affairs will result in the concave-up shape of the tangential velocity at the middle of the channel and the two overshoots in the vicinity of the two disks, which is amply evident in Fig. 5.

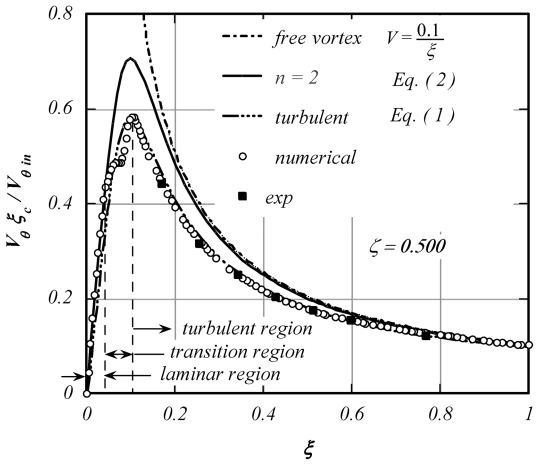

Fig. 6 Tangential velocity distribution along the midchannel plane. The experimental data are taken from Savino and Keshock [13].

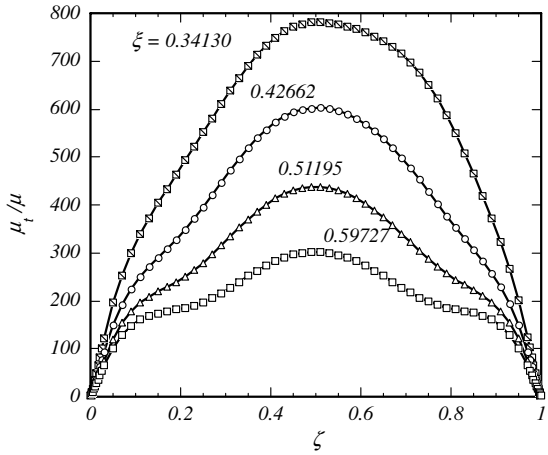

Fig. 7 Normalized turbulent viscosity distributions and location of the maximum turbulent viscosity value.

Returning to Fig. 6, in which the tangential velocity at $\zeta = 0.5$ is given as a function of ξ, we argue that the culprit for the velocity undulation close to the central axis must be turbulence. Near the axis of rotation, the fluid must conform to the laminarlike conditions, evident in every vortex [22]. The azimuth velocity distribution is seen to change modes from turbulent to laminar through a distinct undulation (kink). Referring to Fig. 8, we indeed find the viscosity to posses a similar ripple.

Furthermore, in the radial station $\xi = 0.17065$ (curve A, Fig. 8), the maximum turbulence shifts towards $\zeta = 0$. Accordingly, in Fig. 5, the minimum tangential velocity ζ location is seen to shift in the same direction.

Considering again Fig. 8, we note that in the vicinity of the inlet the flowfield experiences a decreasing level of turbulence that persists up to $\xi \sim 0.8$. Beyond this point, turbulence increases reaching a maximum at about $\xi \sim 0.15$. The last ($\xi \sim 0.8$–0.15) is the region where the toroidal recirculation zone occurs. It is worthy to note in passing that the empirical equation for the apparent viscosity variation provided by Kwok et al.[16], for exactly the same problem, differs radically with the results of the present simulations.

The static pressure for the actual swirling inflow shows a similar behavior as for the hypothetical uniradial sink flow [23]. The turbulent pressure calculations were based on the assumption that the centrifugal acceleration dominates the radial momentum:

$$\frac{V^2}{\xi} = \frac{\mathrm{d}}{\mathrm{d}\xi}\frac{p(r) - p_{\mathrm{in}}}{\rho V_{\theta \mathrm{in}}^2} = \frac{\mathrm{d}\Delta\Pi(\xi)}{\mathrm{d}\xi}$$

Integration of the above equation yields

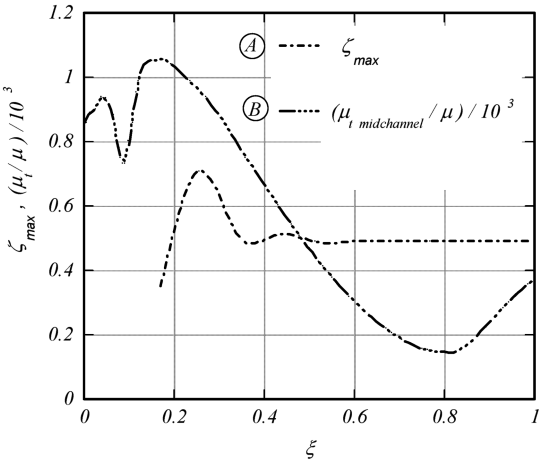

Fig. 8 Turbulent viscosity distributions and location of the maximum turbulent viscosity value.

$$\Delta\Pi(\xi) = \int_0^{\xi} \frac{V^2}{\xi}\,\mathrm{d}\xi + c_o$$

where

$$c_o = \int_0^1 \frac{V^2}{\xi}\,\mathrm{d}\xi$$

Note that c_o actually represents the pressure at the center of rotation.

Inserting the turbulent velocity approximation, we obtain

$$\Delta\Pi(\xi) = 62.88 \int_0^{\xi} \frac{\xi}{\{0.92 + (\frac{\xi}{\xi_c})^4\}^{0.96}}\,\mathrm{d}\xi - 53.90,$$

$$\xi_c = \frac{r_c}{R_o} \approx 0.1$$

The aforementioned integrals are easily evaluated using any of the standard numerical methods, such as Romberg's, or better by using software such as Mathematica, Maple, or MATLAB.

The pressure profile for the $n = 2$ laminar vortex is [21]

$$\Delta\Pi(\xi) = \frac{1}{2\xi_c}\left\{\arctan\left(\frac{\xi}{\xi_c}\right)^2 - \frac{\pi}{2}\right\}$$

The numerical solution of the pressure along with the aforementioned turbulent approximation and that of the $n = 2$ laminar case are shown in Fig. 9. Following the acceleration, which has less effect in the inlet region, pressure drops at a slower pace than in the case of a uniradial flow [23]. However, as it penetrates further into the flow domain, the strong acceleration causes the pressure to experience a considerable plunge, especially near the outlet. Tsifourdaris [24] and Vatistas et al. [25] also reported a similar behavior for the pressure field. The pressure obtained by both the approximate turbulent formulation and the numerical results are in close agreement. The small deviation of the numerical pressure value from the turbulent approximation near the center, evident in Fig. 9, can be explained in the following way. Returning to Fig. 8, we note that the maximum turbulence near the central axis migrates to lower values of ζ and it is therefore no longer at the middle of the channel. The model assumes uniform turbulence with the maximum occurring at $\zeta = 0.5$. Because turbulence at this point is less, the tangential velocity must move toward the laminar $n = 2$. Hence, a more realistic approximation of the pressure must travel in the direction of the $n = 2$ pressure profile. This is precisely what the numerical results are demonstrating.

In the ξ interval ($\sim$0.15, 1), the difference between all the theoretically obtained pressure distributions is relatively small. In this interval, even Rankine's free-forced vortex will provide a tolerable approximation for the pressure. This is the reason behind the reasonable correlation for the static pressure provided by all the past simple models.

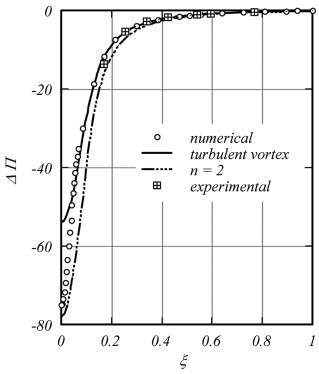

Fig. 9 Radial profile of the static pressure. The experimental data are taken from Savino and Keshock [13].

IV. Conclusions

In this paper we have presented numerical solutions to the steady, incompressible turbulent sink flows that develop between two stationary disks with strong swirl. The method was validated and then we proceeded to elaborate on some key features of the flow. The obtained numerical solutions were in good agreement with past experiments. The centrifugal action was found to be the primary controlling factor. The dominating centrifugal force field guided the fluid to drain through the boundary layers that developed on each disk's surface. The cause for the radial velocity spikes near the disk has been identified and its development has been explained. The commercial numerical algorithm was also able to successfully capture the toroidal recirculation zone that was long known to inhabit the central portion of the flow. This zone, along with the turbulence and the nonslip condition on the disk surface, are responsible for the saddlelike behavior of the tangential velocity. The simulations also unveiled a previously unknown tangential velocity undulation inside the vortex core. The cause of the latter's appearance was attributed to the vortex transition from laminar to turbulent conditions. Therefore, the present study has validated a tool that can now be used to further explore these industrially relevant types of flow.

References

[1] Ragsdale, R. G., "NASA Research on the Hydrodynamics of the Gaseous Vortex Reactor," NASA TND-288, 1960.

[2] Mayer, E. A., and Maker, P., "Control Characteristics of Vortex Valves," *2nd Fluid Amplifier Symposium*, Vol. 2, Diamond Ordnance Fuze Laboratories, Washington, D.C., May 1964, pp. 61–84.

[3] Dahlstrom, D. A., "Cyclone Operating Factors and Capacities on Coal and Refuse Slurries," *Transactions of the American Institute of Mining, Metallurgical and Petroleum Engineers*, Vol. 184, Sept. 1949, pp. 331–344.

[4] Kelsall, D. F., "A Study of the Motion of Solid Particles in a Hydraulic Cyclone," *Transactions of the Institution of Chemical Engineers*, Vol. 30, April 1952, pp. 87–108.

[5] Gupta, A. K., Lilley, D. G., and Syred, N., *Swirl Flows*, Abacus Press, Kent, England, U.K., 1984.

[6] Ranque, G., "Expériences sur la Détente Gigatoire avec Productions Simultanées d'un Echappement d'Air Chaud et d'un Echappement d'Air Froid," *Journal de Physique et le Radium*, Vol. 4, No. 7, 1933, pp. 1123–1158.

[7] Hilsch, R., "Die Expansion von Gasen in Zentrifugalfeld als Kälteprozess," *Z. Naturforsch*, Vol. 1, Feb. 1946, pp. 208–214; also *Review of Scientific Instruments*, Vol. 18, 1947, pp. 108–113. doi:10.1063/1.1740893

[8] Sibulking, M., "Unsteady, Viscous, Circular Flow Part 3. Application to the Ranque–Hilsh Vortex Tube," *Journal of Fluid Mechanics*, Vol. 12, Jan. 1962, pp. 269–298. doi:10.1017/S0022112062000191

[9] Liu, V. C., "A 'Dust Curtain' in Gaseous Core Nuclear Reactors for Rockets," *Nature (London)*, Vol. 226, April 1970, pp. 351–352. doi:10.1038/226351a0

[10] Lewellen, W. S., "A Review of Confined Vortex Flows," NASA CR-1772, July 1971.

[11] Sovran, G., *Fluid Mechanics of Internal Flow*, Elsevier, New York/Amsterdam, 1967.

[12] Vatistas, G. H., "Theoretical and Experimental Studies on Confined Vortex Flows," Ph.D. Thesis, Mechanical Engineering Dept., Concordia Univ., Montreal, 1984.
[13] Savino, J. M., and Keshock, E. G., "Experimental Profiles of Velocity Components and Radial Pressure Distributions in a Vortex Contained in a Short Cylindrical Chamber," NASA TN D-3072, Oct. 1965.
[14] Hornbeck, R. W., "Viscous Flow in a Short Cylindrical Vortex Chamber with a Finite Swirl Ratio," NASA TN D-5132, March 1969.
[15] Wormley, D. N., "An Analytical Model for the Incompressible Flow in Short Vortex Chamber," *Transactions of the American Society of Mechanical Engineers*, Vol. 91, No. 2, June 1969, pp. 264–276.
[16] Kwok, C. C. K., Thinh, N. D., and Lin, S., "An Investigation of Confined Vortex Flow Phenomena," *Transactions of the American Society of Mechanical Engineers. Series D, Journal of Basic Engineering*, Vol. 94, No. 3, Sept. 1972, pp. 689–696.
[17] Sorokin, V. V., "Calculation of Compressible Flow in a Short Vortex Chamber," *Journal of Engineering Physics and Thermophysics*, Vol. 79 No. 5, 2006, pp. 999–1005. doi:10.1007/s10891-006-0196-9
[18] "Fluent 6.1 User's Guide," Fluent, Inc., Lebanon, NH, 2003.
[19] Kendall, J. M., "Experimental Study of a Compressible Viscous Vortex," Jet Propulsion Laboratory, California Institute of Technology, Rept. 32-290, Pasadena CA, June 1962.
[20] Vatistas, G. H., "Simple Model for Turbulent Tip Vortices," *Journal of Aircraft*, Vol. 43, No. 5, 2006, pp. 1577–1579. doi:10.2514/1.22477
[21] Vatistas, G. H., Kozel, V., and Minh, W., "A Simpler Model for Concentrated Vortices," *Experiments in Fluids*, Vol. 11, No. 1, April 1991, pp. 73–76. doi:10.1007/BF00198434
[22] Ramasamy, M., and Leishman, J. G., "Reynolds Number Based Blade Tip Vortex Model," *61st Annual Forum and Technology Display of the American Helicopter Society International*, American Helicopter Society, Alexandria, VA, June 2005.
[23] Vatistas, G. H., "Radial Flow Within Two Flat Disks," *AIAA Journal*, Vol. 28, No. 7, 1990, pp. 1308–1310.
[24] Tsifourdaris, P., "On the Flows Developed Within the Gap of Two Parallel Discs," Ph.D. Thesis, Mechanical and Industrial Engineering, Concordia Univ., Montreal, April 2003.
[25] Vatistas, G. H., Ghaly, W., and Tsifourdaris, P., "Swirling Inflow Within the Narrow Gap of Two Disks," *Journal of Propulsion and Power*, Vol. 21, No. 4, Jul.–Aug. 2005, pp. 743–750.

A. Gupta
Associate Editor